PNAS

Supporting Information for

Structure Making and Breaking in Electrolyte Solutions Explained by Water Energetics.

L. F. Sedano, L. C. Pardo, G. Madrigal, E. G. Noya and C. Vega

cvega@ucm.es

This PDF file includes:

Figs. S1 to S11
Tables S1 to S11
SI References

1. Radial distribution functions

Table S1. Structural properties at 283 K and 1 bar for 1 m lithium, sodium, potassium and cesium chlorides using the Madrid-2019 model (1). Values of the ion-water radial distribution function g_{O-ion} including the positions of the maxima (M) and the minima (m) are collected. The superscripts 1 and 2 indicate the first and second maxima/minima. In parenthesis, we show the value of σ of the LJ potential between the ion and the oxygen atom. CN stands for the coordination number of water in the first hydration shell of the ion.

Pair	$d^{M1}_{g_{O-ion}}$ (Å)	g^{M1}_{O-ion}	$d^{m1}_{g_{O-ion}}$ (Å)	g^{m1}_{O-ion}	$d^{M2}_{g_{O-ion}}$ (Å)	g^{M2}_{O-ion}	$d^{m2}_{g_{O-ion}}$ (Å)	g^{m2}_{O-ion}	CN
O-Li	1.85(2.12)	13.72	2.32	0.0	4.02	1.75	4.84	0.82	4.0
O-Na	2.35(2.61)	7.41	3.25	0.16	4.42	1.51	5.44	0.81	5.5
O-K	2.75(2.89)	4.77	3.56	0.43	4.79	1.22	5.75	0.88	6.6
O-Cs	2.86(3.66)	3.70	3.67	0.56	4.80	1.18	5.88	0.87	6.65
O-Cl	3.06(4.24)	3.74	3.67	0.40	4.76	1.35	5.95	0.83	6.0

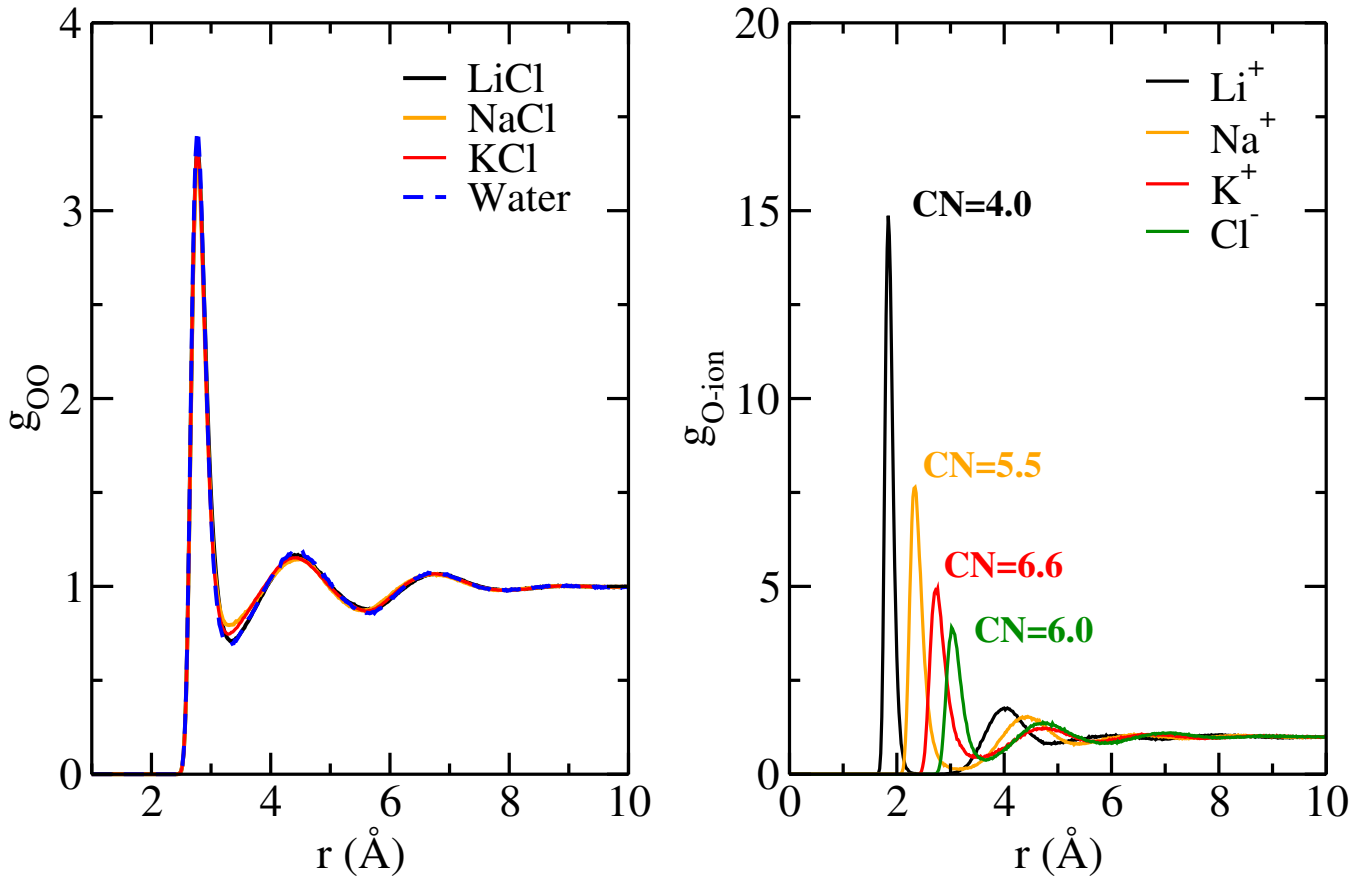

Fig. S1. Radial distribution functions at 283 K and 1 bar for pure water and 1 m electrolyte solutions using the Madrid-2019 model (1).

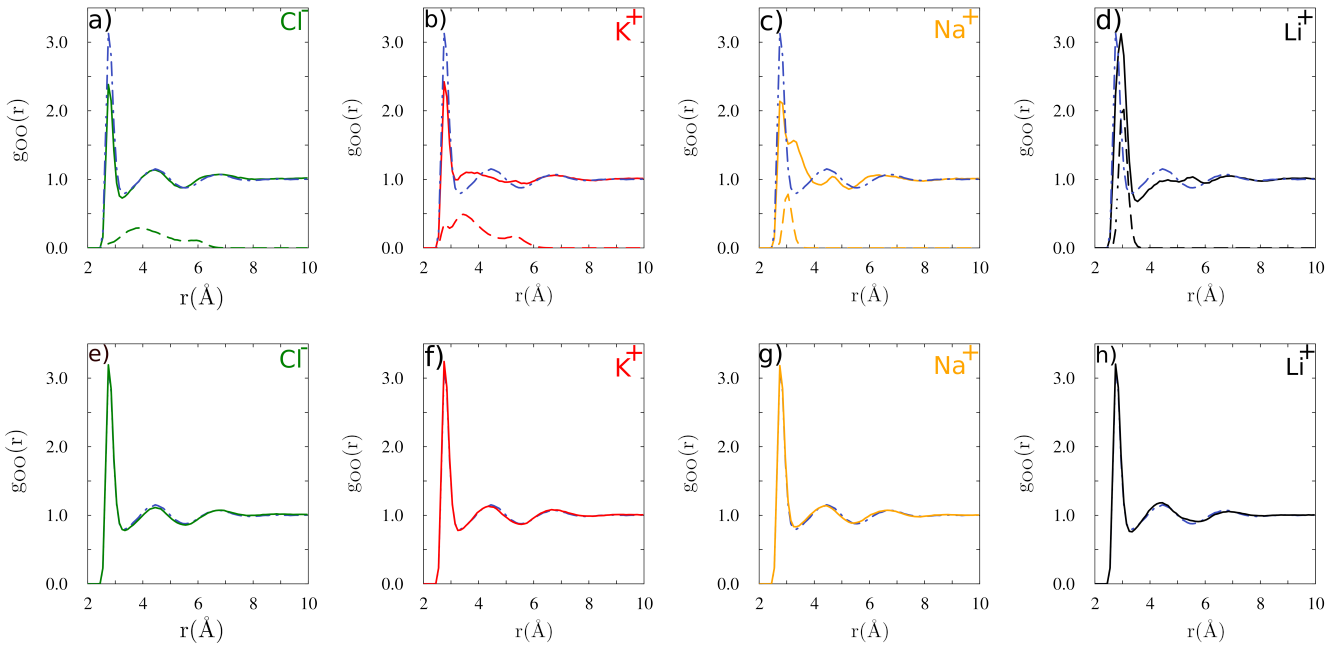

Fig. S2. The Madrid-2019 and TIP4P/2005 models have been simulated at 283 K, 1 bar. Panels a)-d) show oxygen-oxygen radial distribution functions; dashed line: RDF for water molecules that belong strictly to the FHS ($g_{OO}^{hyd-hyd}$). Solid line: RDF for molecules of water in the first hydration shell (FHS) of the ions with the rest of water molecules of the system ($g_{OO}^{hyd-wat}$). In blue colour we show the RDF of pure water. Panels e) - h) show oxygen-oxygen radial distribution functions; solid line: Oxygen-oxygen radial distribution function for molecules of water in the second hydration shell of the ions with the rest of the water molecules of the system. In blue colour we show the RDF of pure water.

2. Angular statistics

The spatial density maps (SDMs) of ions around water were calculated using the ANGULA package (2). The module `cloudXYZ` was employed to transform angular distribution data obtained from the molecular dynamics trajectories into three-dimensional density maps.

From the simulation trajectories, ANGULA generates angular distribution files containing the relative orientations of surrounding ions with respect to a central water molecule, expressed in terms of polar (θ_{pos}) and azimuthal (ϕ_{pos}) angles and, when available, radial distances. The `cloudXYZ` subroutine reads these angular vectors and converts them from spherical to Cartesian coordinates according to:

$$x = d \sin\theta_{pos} \cos\phi_{pos}, \quad y = d \sin\theta_{pos} \sin\phi_{pos}, \quad z = d \cos\theta_{pos}$$

where d is the instantaneous ion–water distance from the trajectory. This yields a point cloud representing the positions of the ions relative to the water molecule across all sampled configurations. To maintain computational efficiency, the number of points can be limited by a user-defined cutoff (typically on the order of 10^5).

The reference frame for the orientation between water molecules is defined by an orthonormal axis set centered on the oxygen atom, as shown in Figure 2 a) of the main text. The Z-axis is aligned with the dipole of the water molecule, i.e., along the bisector of the two hydrogen atoms. The Y-axis is perpendicular to the H–O–H plane (so that the water molecule lies on the XZ plane), and the X-axis is such that $X \times Y = Z$. The XY plane defines the equator of the molecule, while the Z-axis points towards the poles of our reference system. This choice of axis set is crucial to calculate the relative position and orientation between molecules in a meaningful and consistent manner.

The determination of the location and orientation of a molecule with respect to a central one is fully defined by six variables. Three of these correspond to the relative position between molecular centers: the inter-molecular distance r and the two spherical angles ϕ_{pos} and θ_{pos}. We specify here that these two angles are related to the position of a neighbour ion/molecule, since we also calculate the relative orientation of two water molecules. We have decided to drop this subscript in the main text since there is no source of confusion and it eases the reading and visualization of the figures. The other three define the relative orientation between the two molecules, assuming both use the same axis set and correspond to the Euler angles θ_{ori}, ϕ_{ori} and ψ_{ori}, following the Z–Y′–Z″ convention (3). Since this study deals with a disordered system, Probability Distribution Functions (PDFs) of the aforementioned angles are used to identify the most probable configurations. As mentioned in the main text, to avoid the polar-angle dependence of solid angle elements, we calculate the PDFs of azimuthal angles using $\cos(\theta_i)$ instead of θ_i, being i=pos,ori.

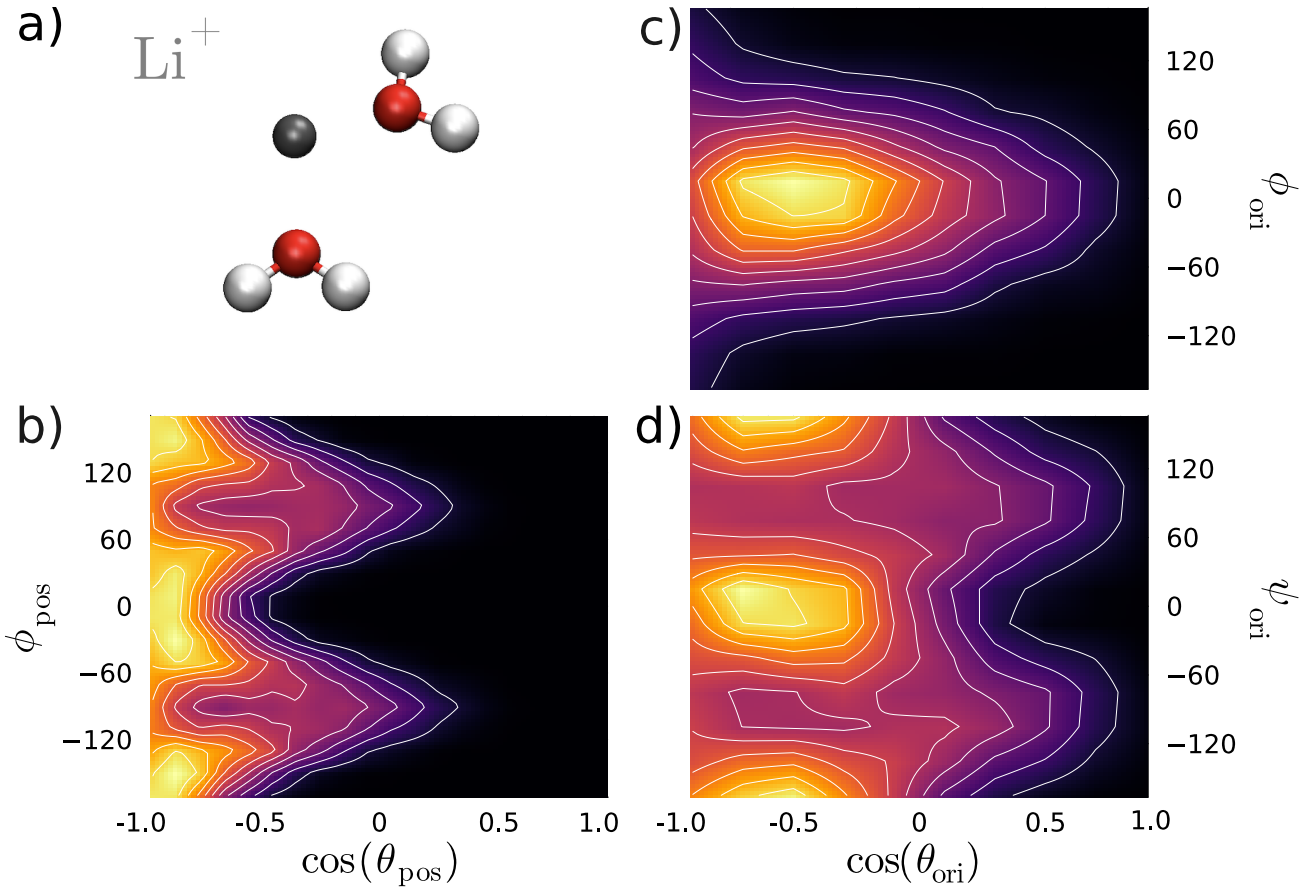

Fig. S3. a) Most probable position and orientation of two water molecules around a central Li^+ cation. b) Positional map PDF$(\cos\theta_{pos}, \phi_{pos})$. In panel c) and d) we show the 2D projections of the orientational maps. High probability regions are shown in yellow colours and blue/black colours show low probability regions for all maps.

We show in Figs. S3,S4,S5 the PDFs describing the relative positions ($P(\cos\theta_{pos}, \phi_{pos})$ and orientation $P(\cos\theta_{ori}, \phi_{ori}, \psi_{ori})$ of two water molecules inside the first coordination shell for distance smaller than 3 Å ($r_{OO} < 3.3$ Å, the minimum of the radial distribution function of water for the TIP4P/2005 model at 283 K 1 bar). In order to determine the orientation, we examine the 2D projections of the full 3D PDFs of the Euler angles. The polar angle is represented by its cosine to ensure equally sized solid angles. The 2D PDFs have been calculated choosing the following binning of the angles:$\Delta\theta_i = 0.1$ and $\Delta\phi_i = \Delta\psi_i = 20^\circ$ being i=pos,ori.

In the case of the Cl^- ion, the most probable position of a water molecule around another one (positional map) can be seen in Figure S5b. We can distinguish in this map the tetrahedral structure of liquid water in the clear spots at $\cos(\theta_{pos}) = 0.6$ and $\phi = 0^\circ, 180^\circ$. A substructure appears around these spots with two clear maxima at $\cos(\theta_{pos}) = 0.6$ and $\phi = \pm 90^\circ$. To calculate the relative orientation, we select the molecules at the locations defined by one of these spots and calculate the Euler angles (the choice of the spot is arbitrary since the two spots appear as a result of molecular symmetry). We show in Figure S5, panels c and d, the orientational maps $PDF(\psi_{ori}, \phi_{ori})$ and $PDF(\psi_{ori}, \cos\theta_{ori})$. The spots are duplicated by the symmetry of the water molecule, as in the positional map.

In the case of the cations, for potassium we were not able to distinguish a clear water structure apart from the tetrahedral one. This fact agrees with the results in the main paper concerning the minimal alteration of the water structure by the largest cation.

Figure S4 shows the results for the Na^+ cation. In panel b, we show the positional map, where we can see a (partial) suppression of the tetrahedral structure of water, indicated by the dark colours in the regions where there should be spots for liquid water (see Figure 4a in the main paper). These spots are replaced by spots at $\cos\theta \approx -0.9$ and $\phi_{pos} = 0^\circ, 180^\circ$. A very marked molecular orientation is seen from the spots in the orientation maps $PDF(\cos\theta_{ori}, \phi_{ori})$ and $PDF(\cos\theta_{ori}, \psi_{ori})$. Putting together the information concerning position and orientation, we show in panel (a) the most probable configuration of two adjoining water molecules around a sodium cation. A very similar result is obtained when performing the same procedure for lithium, as shown in Figure S3, the main difference being that the spots are much better defined and slightly displaced.

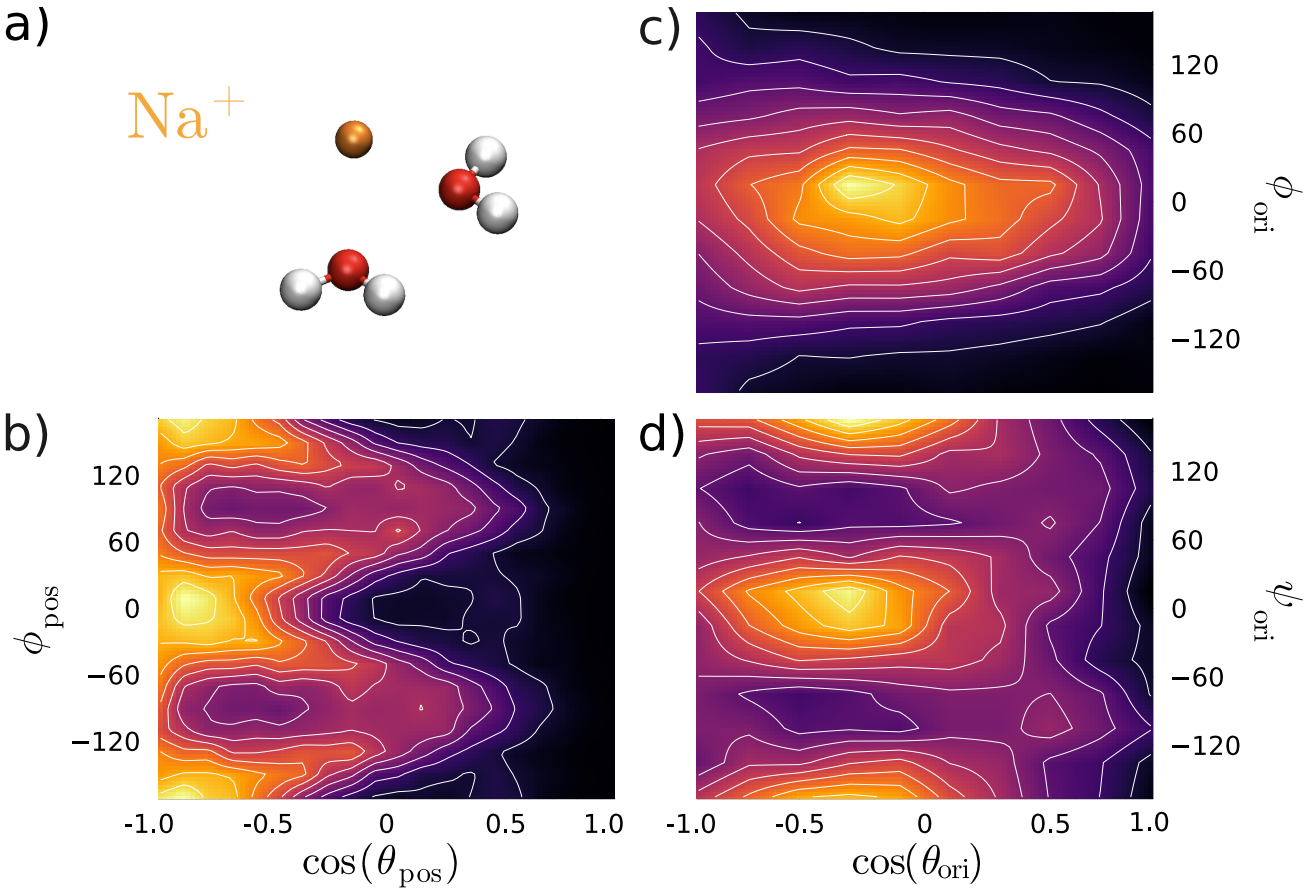

Fig. S4. a) Most probable position and orientation of two water molecules around a central Na^+ cation. b) Positional map $PDF(\cos\theta_{pos}, \phi_{pos})$. In pannels c and d we show the 2D projections of the orientational maps. High probability regions are shown in yellow colours and blue/black colours show low probability regions for all maps.

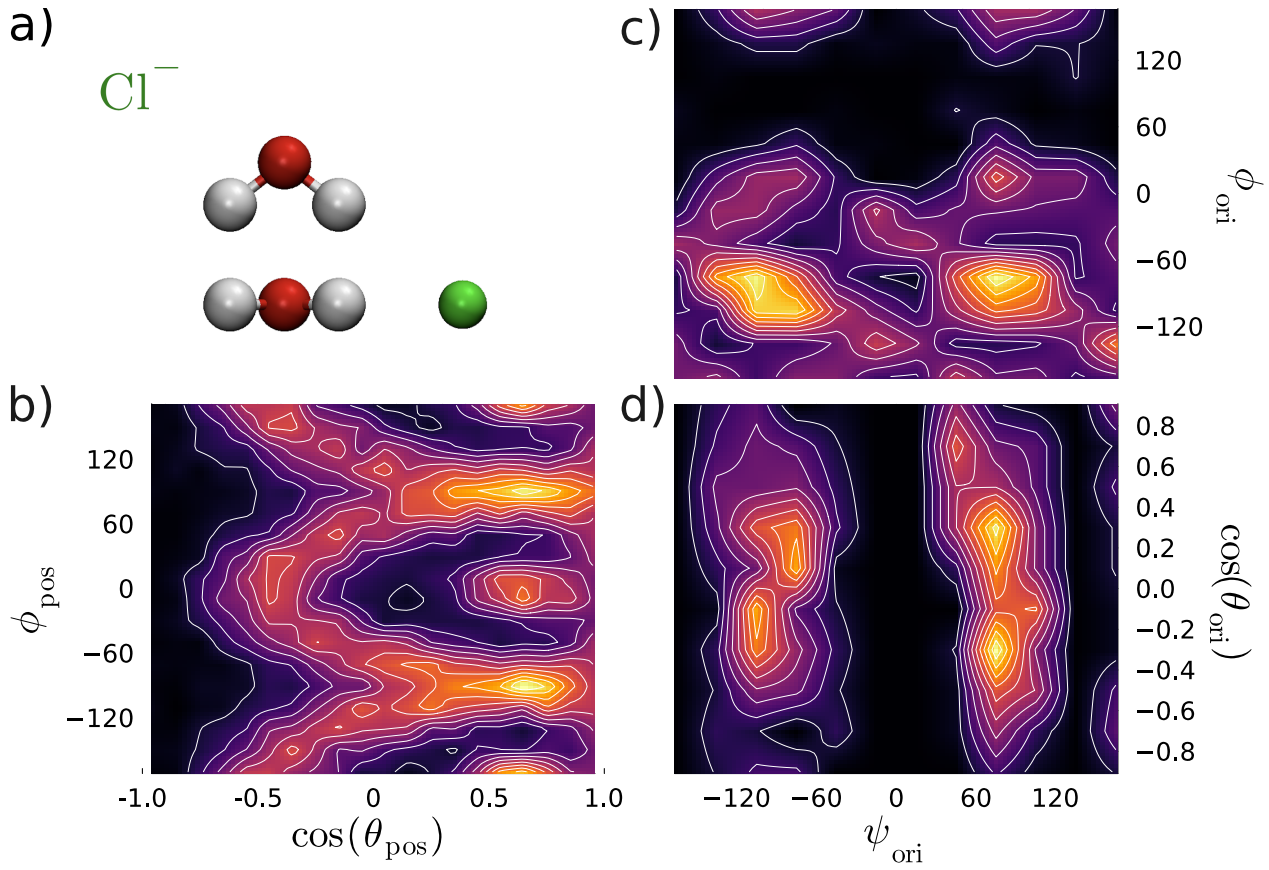

Fig. S5. a) Most probable position and orientation of two water molecules around a central Cl^- ion at distances $d < 3.3$Å. b)Positional map $PDF(\cos\theta_{pos}, \phi_{pos})$. In pannels c and d we show the 2D projections of the orientational maps. High probability regions are shown in yellow colours and blue/black colours show low probability regions for all maps.

A. Spatial Density Map (SDM) Calculation. The position cloud of ions relative to water is processed in VMD (4). An auxiliary Tcl script generated by `cloudXYZ` automates the loading of the coordinates and execution of VMD's `volmap density` command, which bins the ion positions onto a three-dimensional grid of 1.0 Å in each cartesian direction. The volumetric data are exported in OpenDX format (`.dx`) and rendered as isosurfaces in VMD. The calculated isosurfaces represent the three-dimensional probability density distribution of ions around the central water molecule above a certain threshold in density (in % of the maximum density in a voxel), which is specified in Table S2.

Table S2. Threshold of the Spatial Density maps relative to the maximum density in a voxel around a water molecule for the different ions

Ion	Isosurface (%)
Cl^-	52.85
K^+	57.85
Na^+	59.99
Li^+	62.86

3. KL divergence calculation

Information theory has proven to be a very useful tool for investigating molecular ordering at the atomic level (5). Comparison of 2D PDFs, such as those determining the relative molecular position at a given distance ($p(r \mid \phi_{pos}, \cos(\theta_{pos}))$), can be carried out within this theoretical framework using the symmetric version of the Kullback–Leibler divergence (6):

$$D_{\mathrm{KL}}(r) = \sum p(r \mid \phi_{pos}, \cos(\theta_{pos})) \log \frac{p(r \mid \phi_{pos}, \cos(\theta_{pos}))}{q(r \mid \phi_{pos}, \cos(\theta_{pos}))} \quad [1]$$

where $p(r \mid \phi_{pos}, \cos(\theta_{pos}))$ and $q(r \mid \phi_{pos}, \cos(\theta_{pos}))$ are the PDFs associated with the *positional* maps of a water molecule with respect to a central one at a given distance. Since we want to investigate how different is the positional map of bulk water with respect to water in the first hydration shell, $p(r \mid \phi_{pos}, \cos(\theta_{pos}))$ and $q(r \mid \phi_{pos}, \cos(\theta_{pos}))$ correspond to bulk water and to hydration water. The summation is done over all the pixels of the 2D positional maps at the same $(\phi_{pos}, \cos(\theta_{pos}))$ position.

D_{KL} is not generally symmetric, and hence we use its symmetrized version: the average of $D_{\mathrm{KL}}(p, q)$ and $D_{\mathrm{KL}}(q, p)$. For this reason, $p\{x_i\}$ and $q\{x_i\}$ do not have to be unequivocally associated with either bulk water or hydration water. We thus have a way to *unambiguously* determine how similar the two structures are, given that both PDFs are normalized to unity.

For all ions, D_{KL} decreases monotonically up to approximately 2.7 Å, and at larger distances, a pronounced maximum appears in the KL-divergence, being relatively small for chloride and potassium and larger for the other ions coinciding with the additional peak seen in panel c of Figure 3 for sodium between the first and second hydration shells of bulk water and with the high repulsive energy between the FHS water molecules of lithium (Figure 4h). At larger distances, water structure around ions resembles that of bulk water (KL-divergence approaches zero) although for lithium the distortion extends up to $6,$Å.

At first glance, we can see that at short distances correlates with the size of the cations ($D_{\mathrm{KL}}^{Li} > D_{\mathrm{KL}}^{Na} > D_{\mathrm{KL}}^{K}$), with the last one being similar to that of the chloride anion. This is consistent with the qualitative results presented in the main paper and with the calculation of local entropies.

It is worth noting the well-marked double peak at short distances in the case of lithium; this feature matches the two competing structures whose fingerprint is clearly seen in Figure 3h of the main paper, which is less pronounced for the other ions.

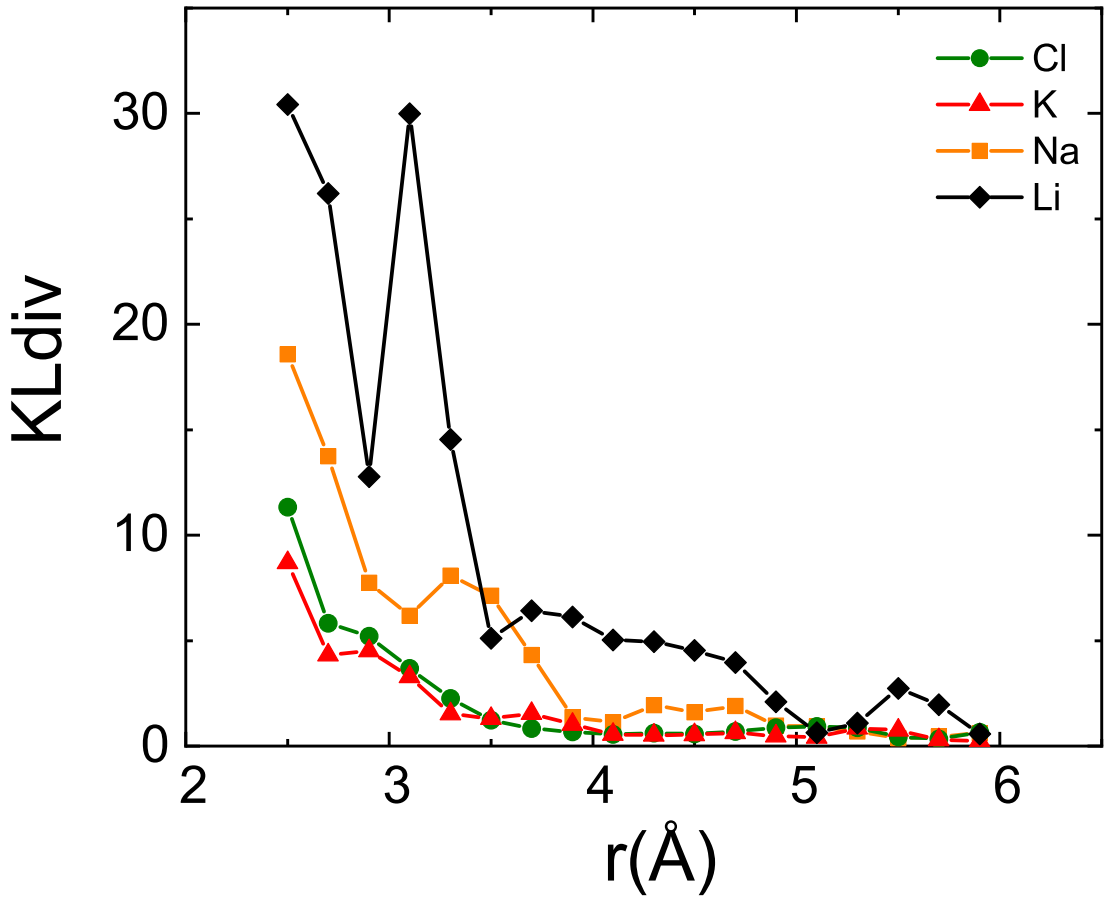

Fig. S6. KL divergence between the positional maps $P(\cos\theta, \phi)$ of bulk water, and water molecules in the first hydration shell of the ions with the rest of the water molecules.

4. Local entropy calculation

We have calculated the excess entropy, taking the ideal gas as a reference ($S^{ex} = S_{liq} - S_{id}$); therefore it is a positive quantity that measures the structure difference of the liquid with respect to that of an ideal gas. We have calculated it using the method described in (5, 7) based on the original decomposition of the entropy proposed by Lazaridis et al. (8). It allows the calculation of excess entropies from the distance-dependent Probability Distribution Functions (PDFs) that describe the position and orientation of a molecule at a given distance to a central one. This approach has the great advantage of being applicable to selected molecules, in our case, those around an ion. By comparing the excess entropy calculated for bulk water with that around the ion, it is possible to obtain a local excess entropy that quantifies how much the local structure of water near ions deviates from that of bulk water.

The total excess entropy can be divided into a translational term calculated from the RDF:

$$S^{ex}_{\text{trans}}(r) = \Big[g_{00}(r)\ln(g_{00}(r)) - g_{00}(r) + 1\Big] 4\pi r^2 \qquad [2]$$

and an angular term calculated from the five angles necessary to completely define the position (polar angles $\cos\theta_{pos}$ and ϕ_{pos}) and the orientation (Euler angles $\cos\theta_{ori}$, ϕ_{ori} and ψ_{ori}) as a function of the distance r to an (arbitrary) central molecule:

$$S^{ex}_{\text{ang}}(r) = \frac{1}{\Omega}\int g(\Omega|r)\ln\big(g(\Omega|r)\big)\mathrm{d}\Omega \qquad [3]$$

where $\Omega = \cos\theta_{pos}, \phi_{pos}, \cos\theta_{ori}, \phi_{ori}, \psi_{ori}$

Once the distance-dependent entropy has been calculated, the total excess entropy is determined by the following equations:

$$S^{\text{ex}}_{\text{trans}} = \frac{1}{2}k\rho\int S_{\text{trans}}(r)\mathrm{d}r \qquad [4]$$

$$S^{\rm ex}_{\rm ang} = \frac{1}{2} k\rho \int S_{\rm ori}(r) g_{OO}(r) 4\pi r^2 {\rm d}r \quad [5]$$

Total excess entropy is simply the summation of all the previous terms:

$$S^{\rm ex} = S^{\rm ex}_{\rm ang} + S^{\rm ex}_{\rm trans} \quad [6]$$

As stated in our previous work (5, 7) a direct calculation of $S^{\rm ex}_{\rm ang}$ has to drawbacks: first the voxels in the 5D-fold PDF of the whole set of angles are sparse leading to an inestable calculation of the entropy, and second a direct calculation does not allow a decomposition between the positional and orientational contributions of the entropy. For this reason we have developed an expansion, based on information theory (5), of the angular entropy. We recall here the main definitions for the sake of clarity. $S_{\rm ang}(r)$ can be expanded in mutual information and entropy terms up to third order:

$$S^{(5)}(r) = \sum S^{(1)}(r) - \sum I^{(2)}(r) + \sum I^{(3)}(r) + \mathcal{O}(4),$$

where the superscript (i) on the mgnitudes indicates the number of variables of a given PDF. For two angles A and B $(i = 2)$:

$$I(A, B) = S(A) + S(B) - S(A, B),$$

and similarly for three variables.

The positional entropy contribution, that related with the PDF of the variable θ_{pos} and ϕ_{pos} describing the position of a molecule with respect to a central one, is defined as:

$$S_{\rm pos}(r) = S(\theta_{\rm pos}|r) + S(\phi_{\rm pos}|r) - I(\theta_{\rm pos}, \phi_{\rm pos}|r),$$

and the orientational part, that related with the PDF of the variables θ_{ori},ϕ_{ori} and ψ_{ori} describing the orientation of a molecule with respect to a central one:

$$\begin{aligned} S_{\rm ori}(r) =& S(\theta_{\rm ori}|r) + S(\phi_{\rm ori}|r) + S(\psi_{\rm ori}|r) \\ & - I(\theta_{\rm ori}, \phi_{\rm ori}|r) - I(\theta_{\rm ori}, \psi_{\rm ori}|r) - I(\phi_{\rm ori}, \psi_{\rm ori}|r) \\ & + I(\theta_{\rm ori}, \phi_{\rm ori}, \psi_{\rm ori}|r). \end{aligned}$$

Finally, the cross-term is given by:

$$S_{\rm pos,ori}(r) = S_{\rm ang}(r) - S_{\rm pos}(r) - S_{\rm ori}(r)$$

5. Hydrogen bonding

Table S3. Average number of hydrogen bonds according to the Luzar-Chandler criterium (9) (see main text) for 1 m solutions using the Madrid-2019 (1) at 298.15 K and 1 bar. Pure water (TIP4P/2005) has 3.57 HB. The superscript *FHS* indicates the HB formed between water molecules belonging to the first hydration shell of an ion with each other and *free* is the HB formed by water molecules that are not hydrating any ion with any other water molecule. Superscripts "+" and "-" correspond to the cation and anion.

	LiCl	NaCl	KCl	CsCl	LJ$_{KCl}$
n$_{HB}$	3.37	3.36	3.37	3.37	3.57
n$^{free}_{HB}$	3.56	3.56	3.56	3.56	3.56
n^{+}_{HB}	2.12	2.30	2.54	2.60	3.58
n^{-}_{HB}	2.56	2.54	2.54	2.54	3.55
$n^{FHS,+}_{HB}$	0	0.27	1.32	1.43	10.8
$n^{FHS,-}_{HB}$	0.28	0.28	0.28	0.26	14.5

Table S4. Average number of hydrogen bonds according to the Luzar-Chandler criterium (9) (see main text) for 1 m solutions using the Madrid-2019 (1) at 283 K and 1 bar. Pure water (TIP4P/2005) has 3.63 HB. The superscript *free* corresponds the HB formed by water molecules that are not hydrating any ion with any other water molecule. Superscripts "+" and "-" indicate cation and anion, respectively.

	Donor				Acceptor			
	LiCl	NaCl	KCl	CsCl	LiCl	NaCl	KCl	CsCl
n$_{HB}$	1.72	1.72	1.72	1.72	1.72	1.72	1.72	1.72
n$^{free}_{HB}$	1.81	1.82	1.82	1.82	1.82	1.83	1.82	1.82
n^{+}_{HB}	1.74	1.66	1.66	1.68	0.43	0.70	0.93	0.97
n^{-}_{HB}	0.90	0.90	0.90	0.89	1.71	1.70	1.69	1.70

Table S5. Average number of hydrogen bonds according to the Luzar-Chandler criterium (9) (see main text) for 1 m solutions using the Madrid Transport (10) at 283 K and 1 bar. Pure water (TIP4P/2005) has 3.63 HB. The superscript *free* corresponds the HB formed by water molecules that are not hydrating any ion with any other water molecule. Superscripts "+" and "-" indicate cation and anion, respectively.

	Donor				Acceptor			
	LiCl	NaCl	KCl	CsCl	LiCl	NaCl	KCl	CsCl
n_{HB}	1.69	1.68	1.68	1.69	1.69	1.68	1.68	1.69
n_{HB}^{free}	1.77	1.78	1.77	1.78	1.78	1.79	1.79	1.78
n_{HB}^{+}	1.71	1.62	1.63	1.64	0.41	0.67	0.91	0.95
n_{HB}^{-}	0.88	0.88	0.89	0.88	1.68	1.66	1.65	1.66

6. Energy calculations

The heat maps of Figure 3 (main text) have been calculated by performing a two-dimensional Probability Distribution Function (PDF) using a grid of distance to a central molecule versus energy, with $\Delta r = 0.1$ and $\Delta E = 1$ kJ/mol. The PDF was then rescaled by the volume of the spherical shell to normalize all pixels at a given distance to one neighbour molecule, i.e., the PDF values were divided by $4\pi r^2 \Delta r$. For clarity of the figure, we further divided the PDF by its maximum value, so that the contour lines represent a fixed percentage with respect to the maximum of the function in all cases.

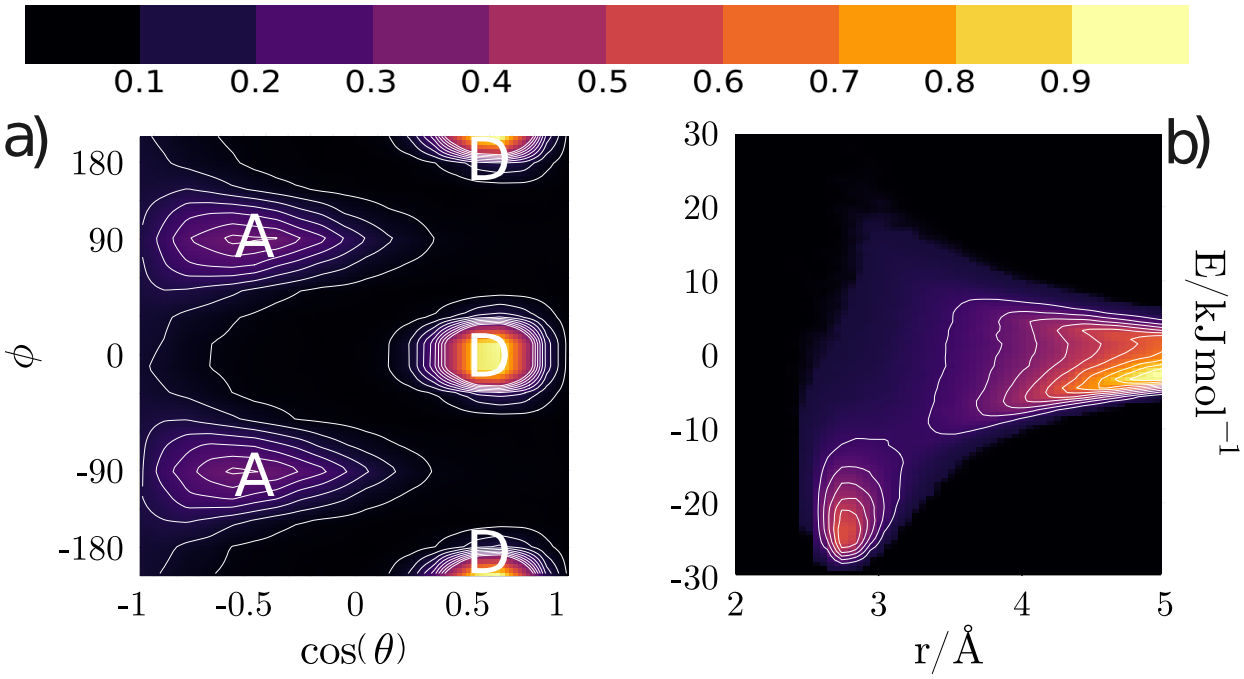

Fig. S7. Bivariate distribution function of the energy for TIP4P/2005 water at 283 K.

GROMACS allows the selection of energy groups for computing pair energies contributions. However, in systems with coulombic interactions, the reciprocal space contribution of the PME method is treated collectively, and it is not possible to break down the energy into groups. Therefore, to calculate the ion-ion energy, we extract only the positions of the ions from the trajectory of the electrolyte solution (which uses PME) and compute the ion-ion energies by including both the LJ and the coulombic contribution (using PME for the coulombic interactions). The water-water energy is evaluated analogously by removing the ion positions from the trajectory. Finally, the water-ion energies are obtained by subtracting the ion-ion and water-water contributions from the total energy.

In the post-analysis for computing the contributions to the energy (see Section *The impact of ions on the water potential energy* in the main text), when showing how the water-water energy changes as a function of the interaction cutoff distance (Fig 5 in the main text), the trajectories were reanalyzed by removing the ions and evaluating directly the water-water energy including both the LJ and the coulombic contribution (without using PME).

Table S6. Contribution of water-water interactions to the potential energy (u_{ww}) for pure water and 1 m solutions at 283 K (1 bar) with the Madrid-Transport model (q=0.75) (10).

	$u_{ww}(kJ/mol)$	% Δu_{ww} (kJ/mol)
Pure Water (U^0_{ww})	-48.84	-
LiCl	-41.88	14.25
NaCl	-42.52	12.93
KCl	-43.02	11.92
CsCl	-43.13	11.68

Table S7. Contribution of water-water interactions to the potential energy (u_{ww}) for pure water and 1 m solutions at 298.15 K (1 bar) with the Madrid-2019 model (q=0.85) (1) and the Madrid-Transport model (q=0.75) (10).

	$u_{ww}(kJ/mol)$	% Δu_{ww} (kJ/mol)
Pure Water	-47.86	
	Madrid-2019	
LiCl	-40.14	16.12
NaCl	-40.51	15.35
KCl	-41.20	13.91
CsCl	-41.36	13.57
$MgCl_2$	-28.77	39.88
$CaCl_2$	-30.59	36.09
	Madrid Tansport	
LiCl	-40.96	14.44
NaCl	-41.61	13.09
KCl	-42.12	12.02
CsCl	-42.20	11.85
$MgCl_2$	-31.39	34.41
$CaCl_2$	-33.17	30.70

Table S8. Ions-water potential energy (in kJ/mol) for the different 1 m salt solutions at 298.15 K and 1 bar for the Madrid-2019 model.

	u_{w-ions}(kJ/mol$_{water}$)	u_{w-ions}(kJ/mol$_{salt}$)
LiCl (aq)	-17.3	-967.4
NaCl (aq)	-15.0	-832.5
KCl (aq)	-13.1	-726.5
CsCl (aq)	-12.2	-676.0
$MgCl_2$	-46.1	-2560
$CaCl_2$	-39.0	-2163

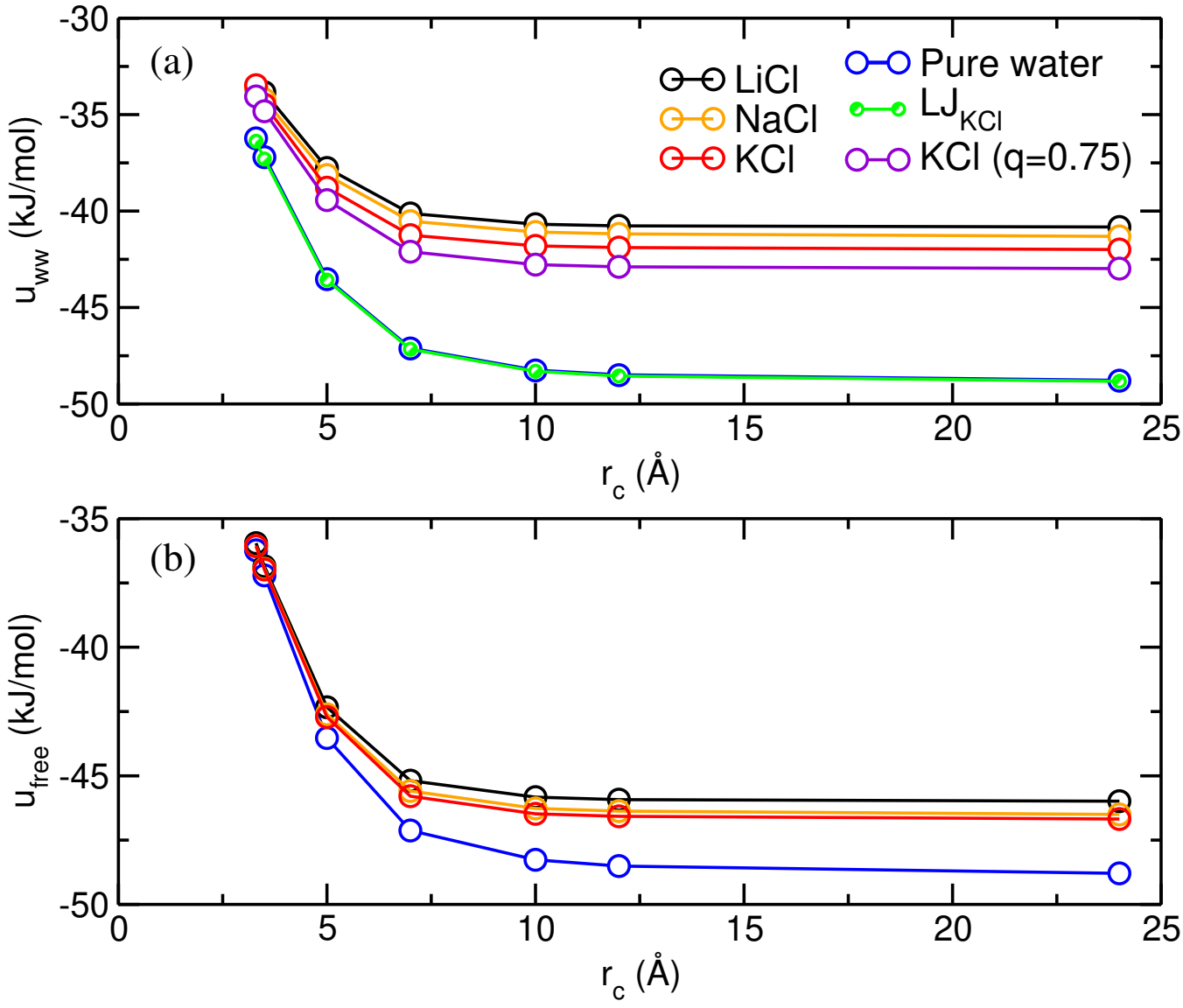

Fig. S8. a) Water-water energy (see Eq. 1 of the main text) as a function of the cut-off distance for the interaction potential at 283 K and 1 bar for 1 m solutions using the Madrid-2019 model (1) and Madrid Transport (q=0.75) (10). b) Free water energy (see Eqs. 2 and 3) compared to the energy of pure water (colors follow the legend of panel (a)).

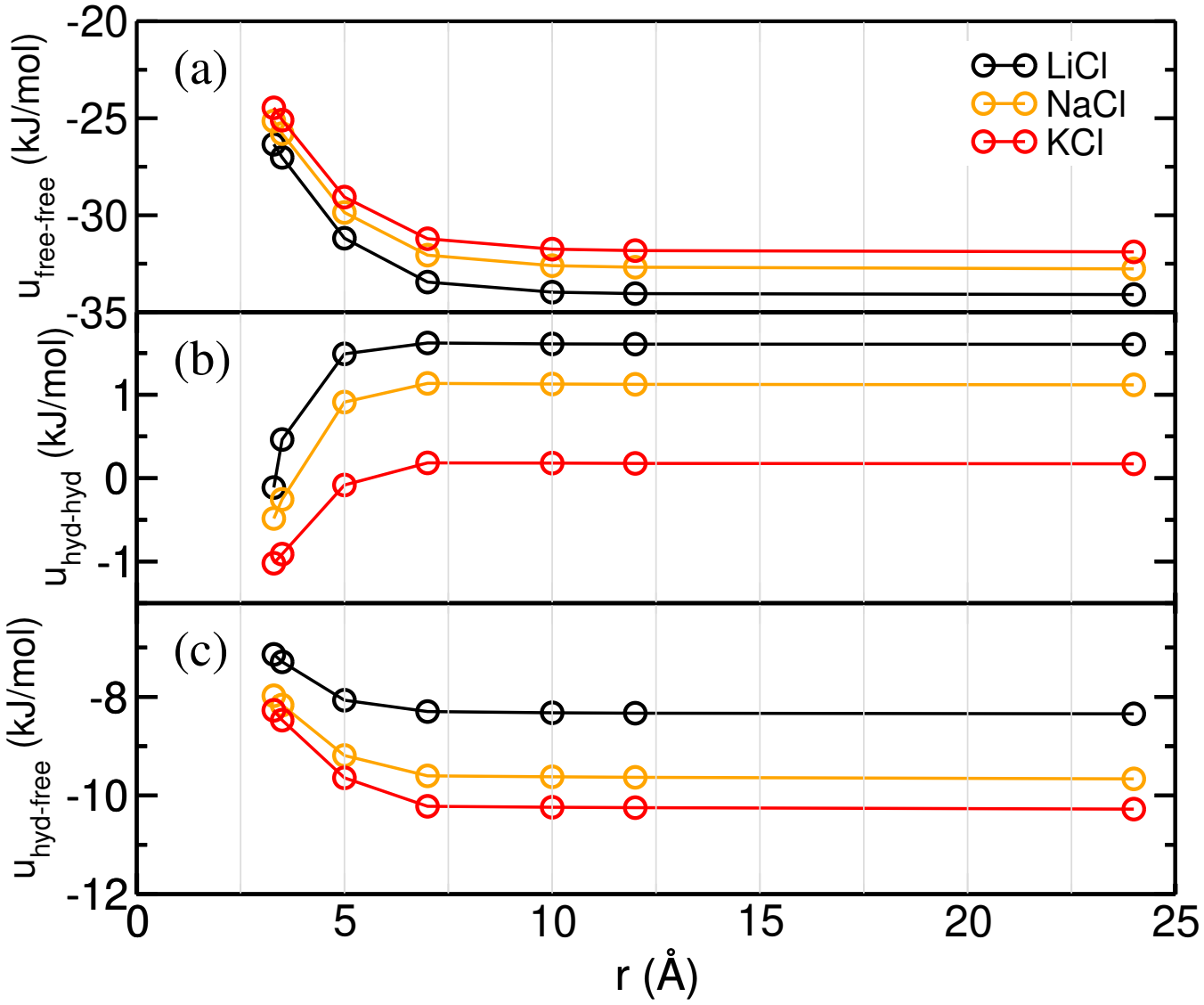

Fig. S9. Energy contributions from hydrated and free water molecules as defined in Eq. 1 of the main text using the Madrid-2019 (1) model at 283 K and 1 bar.

7. Viscosity

The Jones Dole equation describes quite well the variation of the viscosity of electrolyte solutions:

$$\eta/\eta_w = 1 + A\sqrt{m} + Bm + Cm^2 + ... \quad [7]$$

where η is the viscosity of the solution at molality m and η_w is the viscosity of pure water. The coefficient A is always positive and rather small. It can be estimated quite well from a theoretical expression that uses transport properties of the ions in water at infinite dilution (11). The term A is at least one order of magnitude smaller than B. If neglected, and at moderate concentrations, B can be regarded as a constant proportional to the change of the viscosity of the solution compared to that of pure water. For some salts, B has been found to be negative; that is, the solution becomes less viscous than pure water. The term A captures the viscosity change due to Coulombic ion-ion interactions, term B, that from ion-water interactions, and term C represents the interactions between hydrated ions. At low concentrations, the quadratic contribution can be neglected and Eq. 7 can be rewritten as:

$$(\eta/\eta_w - 1)/\sqrt{m} = A + B\sqrt{m} \quad [8]$$

Thus, a fit of the term on the left hand side as a function of $\sqrt{m}$ should be linear. This is the way the coefficients A and B are obtained in experiments. The experimental uncertainty of B is typically around 0.01 (12). Determining A and B from simulations is a *tour of force*, as it requires extremely long simulations to estimate the viscosity with very high accuracy at low concentrations. In fact, there is only one paper in the literature (13) with a rigorous evaluation of the Jones-Dole coefficients for some force fields of 1:1 electrolytes. In that work, B coefficients were obtained by fitting the simulation results for concentrations between 0.1 and 1 m, while the values of A were not reported since the associated statistical error was larger than the absolute values. In this work, we estimate the B coefficients by using the expression:

$$B' \simeq (\eta/\eta_w - 1 - A\sqrt{m})/m \quad [9]$$

Given that $A << B$, we take the experimental values of A to obtain B'. These are ≈ 0.005 for 1:1 and ≈ 0.02 for 2:1 electrolytes (12). To evaluate B', a concentration such that the quadratic term contribution in the Jones-Dole equation (Eq. 7) can be neglected is needed. For 1:1 electrolytes at 1 m, only 1-2% of the ions share a water molecule in their hydration shell (see main text), which ensures a small contribution of C to Eq. 7. For 2:1 electrolytes, we use a concentration of 0.6 m to keep the total number of ions similar. To check the validity of Eq. 9 as an approximate way of estimating B, we have followed the procedure described above using experimental values of the viscosity (14, 15). For the specific case of $MgCl_2$, the viscosity at 0.6 m was not available from Ref. (14), so we opted to evaluate the experimental B' at 0.5 m for this salt. In Table S9, the resulting values of B' show excellent agreement with those reported by Marcus (11). The typical difference is of about 0.01, which coincides with the associated experimental uncertainty of B.

Table S9. B' coefficients at 298.15 K obtained by applying Eq. 9 to experimental viscosities (14, 15). The experimental values of B are taken from Ref. (11). ΔB is defined as $B' - B_{exp}$.

Salt	Viscosity (mPa·s)	B' (kg/mol)	B_{exp} (kg/mol)	ΔB (kg/mol)
LiCl	1.022	0.15	0.14	0.01
NaCl	0.974	0.09	0.08	0.01
KCl	0.888	0.00	-0.01	0.01
CsCl	0.857	-0.04	-0.05	0.01
$MgCl_2$	1.075	0.39	0.38	0.01
$CaCl_2$	1.060	0.29	0.29	-0.00

For the viscosity calculations, we run 24 independent simulations in the NVT ensemble (keeping the rest of the simulation details specified in the main text) of 20 ns each (i.e., we used in total 480 ns to determine the viscosity of one salt and force field). The volume used in the NVT simulations was obtained from a NpT run of 20 ns. The system contains 4440 molecules of water and the number of ions needed for the required concentration. Our estimated uncertainty for B' is 0.04 kg/mol (obtained from the standard deviation from the viscosity seeds). The viscosity of TIP4P/2005 water at 298.15 K and 1 bar is 0.866(3) mPa $\cdot$ s (the experimental one is 0.890 mPa $\cdot$ s). Results for the viscosities and for the B' coefficients are presented in Table S10 for the Madrid-2019 (1) (q=0.85) and for the Madrid-Transport (q=0.75) (10) models. The latter had parameters only for Cl^-, Na^+ and K^+. In this work, we have extended the model (see next section).

Finally, we discuss in the main text that two trends are observed for monovalent and divalent ions when the attention is focused on the water-water interaction energy of solutions. This is precisely the trend observed for the partial molar entropies measured by Lattimer (17). Fig. 6 from the main text is displayed along with these entropies in Fig. S10.

Table S10. Viscosities and B' coefficients (see Eq. 9) at 298.15 K for the Madrid-2019 (1) and Madrid Transport (10), which has been extended in this work (see Table S11 for the parameters). The experimental values of B are taken from Ref. (11). ΔB is defined as $B' - B_{exp}$. The viscosity of pure water for TIP4P/2005 is 0.866 mPa·s (close to the experimental value of 0.890). The viscosities of the Madrid-2019 and Madrid-Transport force fields were computed at 1 m for 1:1 electrolytes and at 0.6 m for $MgCl_2$ and $CaCl_2$.

Salt	Viscosity (mPa·s)		B' (kg·mol^{-1})			
	2019	Transport	2019	ΔB^{2019}	Transport	ΔB^{t}
LiCl	1.060	0.964	0.22	0.08	0.11	-0.03
NaCl	1.023	0.981	0.18	0.10	0.13	0.05
KCl	0.945	0.899	0.09	0.10	0.03	0.05
CsCl	0.941	0.904	0.08	0.13	0.04	0.09
$MgCl_2$	1.137	1.070	0.50	0.12	0.37	-0.01
$CaCl_2$	1.082	1.045	0.39	0.10	0.32	0.03

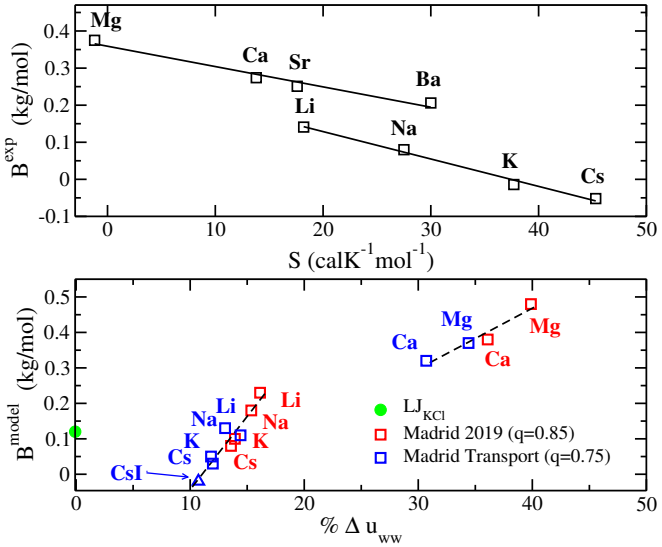

Fig. S10. Top: Partial molar entropies at 298.15 K of chloride salts taken from Ref. (16) (page 173, Tabl 25). Bottom: Jones-Dole viscosity coefficient at 298.15 K (see Eq. 7 for the two models studied in this work (1, 10) as indicated in the legend and for the LJ_{KCl} particle (see text) *vs* the percentage of the energy loss of water-water interactions in the solution compared to pure water (see Eq. 1 in main text). Black lines are fits using the data of both models for monovalent and divalent solutions. Chlorides are represented by squares. The cesium iodide is indicated by a triangle. Red symbols: Madrid-2019. Blue symbols: Madrid-transport.

8. Parameters of the Madrid-Transport and the LJ_{KCl} particle

As mentioned in the main text, the Madrid-Transport(10) was developed based on the observation that a reduced formal charge on ions provided better transport properties (i.e., diffusion, viscosity and electrical conductivity) (18). For the purpose of comparing the B coefficient with the energy of water in solution, we have extended the model to other ions; namely Li^+, Cs^+, Mg^{2+}, Ca^{2+} and I^-. The densities as a function of the concentration of the new model are presented in Fig. S11, and the parameters can be found in Table S11.

Finally, an hydrophobic particle denoted as LJ_{KCl} has been used in this work to study separately the columbic and the volume effects perpetrated by ions. This is implemented by simulating the Madrid-2019 force field of KCl and assigning zero charge to both K and Cl and modifying the value of σ for the Cl-O interaction to 0.328 nm, and the value of σ for the K-O interaction to 0.2415 nm. The resulting LJ particle replicates the K-O and Cl-O distances (i.e., the first maximum of the radial distribution function) from the original Madrid-2019 force field for KCl. The viscosity was calculated at 1 m, 298.15 K and 1 bar, yielding a value 0.967 mPa.s. The resulting B' is 0.117 (note that the term A is not used for the non-ionic system).

Table S11. Parameters for the extension of the Madrid-Transport model (10). All ions have a charge of $\pm$ 0.75 (divalent cations +1.5). The ion-ion parameters are taken from Ref. (10) for Na, K and Cl. For cation-cation and anion-anion interactions, the parameters were taken from Ref. (1).

		σ (nm)	ϵ (kJ/mol)
Li	Li	0.14397	0.43509
Li	O	0.18450	0.70065
Li	Cl	0.27000	1.28294
Na	Na	0.22174	1.47236
Na	O	0.23873	0.79339
Na	Cl	0.25801	1.43889
K	K	0.23014	1.98574
K	O	0.28954	1.40043
K	Cl	0.34170	1.40000
Cs	Cs	0.35210	0.375960
Cs	O	0.36000	0.10000
Cs	Cl	0.43185	0.16156
Cs	I	0.44379	0.24645
Mg	Mg	0.11629	3.65190
Mg	O	0.18025	12.0000
Mg	Cl	0.30000	3.00000
Ca	Ca	0.26656	0.50720
Ca	O	0.23900	7.25000
Ca	Cl	0.31500	1.00000
Cl	Cl	0.46991	0.07692
Cl	O	0.40763	0.06198
I	I	0.50498	0.179010
I	O	0.43495	0.100000

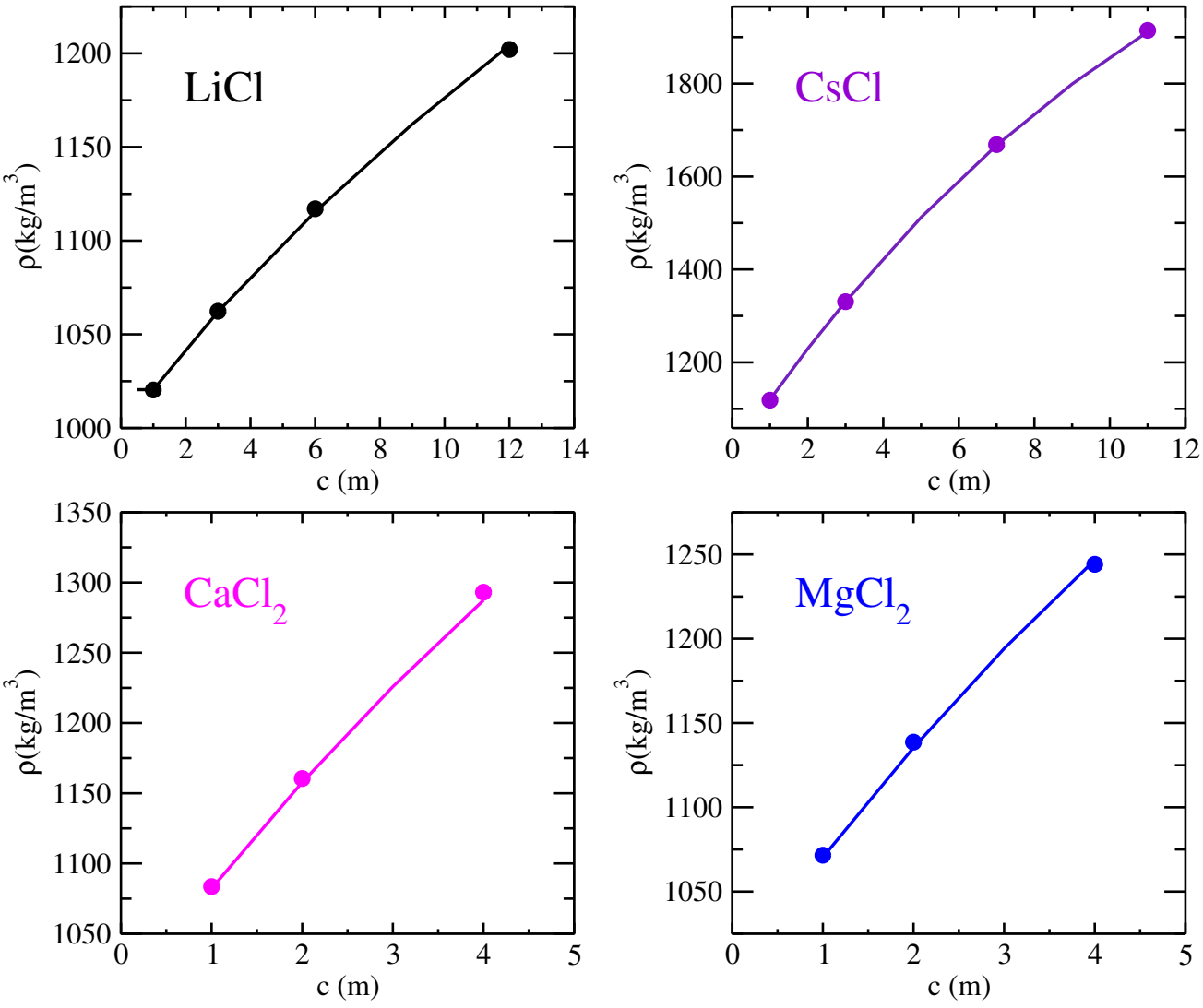

Fig. S11. Density as a function of concentration at 298.15 K and 1 bar for the salts of the Madrid-Transport developed in this work. Symbols are simulation results and solid lines are experimental densities from Ref. (19). CsI has only been determined at 1 m yielding a density of 1183 kg/m^3 (the experimental one is 1186 kg/m^3).

References

1. I Zeron, JLF Abascal, C Vega, A force field of Li^+, Na^+, K^+, Mg^{2+}, Ca^{2+}, Cl^-, and SO_4^{2-} in aqueous solution based on the TIP4P/2005 water model and scaled charges for the ions. *J. Chem. Phys.* **151**, 134504–16 (2019).
2. LC Pardo, ANGULA (https://gcm.upc.edu/en/members/luis-carlos/angula) (2010) Software.
3. H Goldstein, CP Poole, JL Safko, *Classical Mechanics*. (Addison Wesley, San Francisco), Third edition edition, (2002).
4. W Humphrey, A Dalke, K Schulten, Vmd: visual molecular dynamics. *J. molecular graphics* **14**, 33–38 (1996).
5. LC Pardo, A Henao, A Vispa, Characterizing ordering in liquids: An information theoretic approach. *J. Non-Cryst. Solids* **407**, 220–227 (2015).
6. A Henao, D Angulo-García, GJ Cuello, P Negrier, LC Pardo, Investigating disordered phases of c2cl6 using an information theory approach. *J. Mol. Liq.* **362**, 119708 (2022).
7. A Henao, S Busch, E Guàrdia, JL Tamarit, LC Pardo, The structure of liquid water beyond the first hydration shell. *Phys. Chem. Chem. Phys.* **18**, 19420–19425 (2016).
8. T Lazaridis, M Karplus, Orientational correlations and entropy in liquid water. *The J. Chem. Phys.* **105**, 4294–4316 (1996).
9. A Luzar, D Chandler, Hydrogen-bond kinetics in liquid water. *Nature* **379**, 55 (1996).
10. S Blazquez, MM Conde, C Vega, Scaled charges for ions: An improvement but not the final word for modeling electrolytes in water. *The J. Chem. Phys.* **158**, 054505 (2023).
11. Y Marcus, *Ion Properties*. (Marcel Dekker, Inc.), (1997).
12. HDB Jenkins, Y Marcus, Viscosity b-coefficients of ions in solution. *Chem.Rev.* **95**, 2695 (1995).
13. S Yue, AZ Panagiotopoulos, Dynamic properties of aqueous electrolyte solutions from non-polarisable, polarisable, and scaled-charge models. *Mol. Phys.* **117**, 3538–3549 (2019).
14. M Laliberté, Model for calculating the viscosity of aqueous solutions. *J. Chem. Eng. Data* **52**, 321–335 (2007).
15. T Nakai, S Sawamura, Y Taniguchi, Effect of pressure on the viscosity of aqueous cesium chloride solution at 25 c. *J. Molec. Liq.* **65/66**, 365–368 (1995).
16. RW Gurney, *Ionic Processes in Solution*. (McGraw Hill, New York), (1953).
17. W Latimer, KS Pitzer, WV Smith. *J. Am. Chem. Soc.* **60**, 1831 (1938).
18. S Blazquez, et al., Computation of electrical conductivities of aqueous electrolyte solutions: Two surfaces, one property. *J. Chem. Theory Comput.* **19**, 5380–5393 (2023).
19. M Laliberte, WE Cooper, Model for calculating the density of aqueous electrolyte solutions. *J. Chem. Eng. Data* **49**, 1141–1151 (2004).